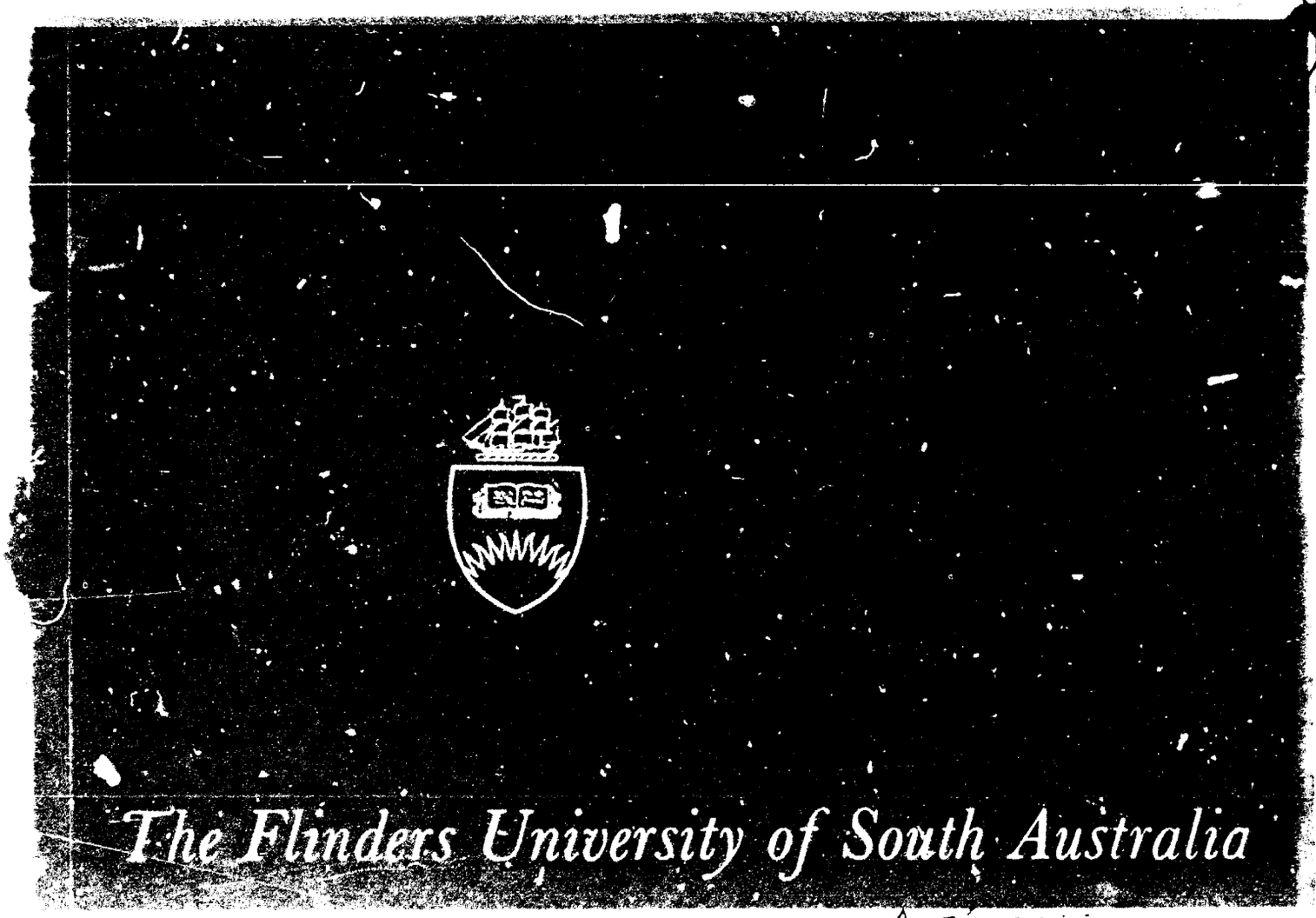

AU76

(e,2e) SPECTROSCOPY OF ETHANE

S. DEY, A.J. DIXON, I.E. McCARTHY and E. WEIGOLD

FIAC-R-5

APRIL 1976

(e,2e) SPECTROSCOPY OF ETHANE

S. Dey, A.J. Dixon, I.E. McCarthy and E. Weigold
School of Physical Sciences,
The Flinders University of South Australia,
Bedford Park, S.A., Australia 5042

ABSTRACT

The 400eV and 1200eV noncoplanar symmetric (e,2e) reaction has been used to measure the momentum distributions of electrons in the individual valence orbitals of ethane as well as to measure the complete separation energy spectra in the valence region. The shapes and relative magnitudes of the momentum distributions agree well with those calculated using the plane wave off-shell impulse approximation and double zeta basis molecular orbital wave functions. The ground state of $C_2H_6^+$ is shown to be $1e_g^{-1}$ with the vertical ionization potential being 12.25 ± 0.1 eV. Considerable structure due to configuration interaction is observed in the separation energy region 29eV to 55eV. Much of this structure can be assigned to the $2a_{1g}$ orbital.

1. INTRODUCTION

The electronic structure of ethane is interesting for a number of reasons. Firstly the C_2H_6 molecule is normally considered as the prototype for the single carbon-carbon bond as well as a prototype for tetrahedral (sp^3) hybridization. Secondly there has been some controversy over the nature of the ground electronic state of $C_2H_6^+$.

The electronic structure of methane, which is often taken as another example of tetrahedral hybridization, has been investigated in some detail using the (e,2e) technique[1,2]. The joining of the two methyl groups to form ethane removes the degeneracy of the $1t_2$ orbital of methane, which splits into three orbitals ($1e_g$, $3a_1$ and $1e_u$), and of the $2a_1$ orbital of methane which splits into two ($2a_{2u}$ and $2a_{1g}$).

Molecular orbital calculations[3-7] predict that the ground state electronic configuration for ethane should be

$$(1a_{1g})^2\ (1a_{2u})^2\ (2a_{1g})^2\ (2a_{2u})^2\ (1e_u)^4\ (3a_{1g})^2\ (1e_g)^4\ {}^1A_{1g}, \qquad (1)$$

the point group for the molecule being D_{3d}, the staggered configuration being more stable than the eclipsed configuration.

This electronic configuration suggests that the ground state of $C_2H_6^+$ should be ^2E_g corresponding to the $1e_g^{-1}$ configuration. However, some recent ab initio MO calculations[8,9] have for different reasons predicted that the ground ionic state should be $^2A_{1g}$, corresponding to the $3a_{1g}^{-1}$ configuration, rather than ^2E_g. The MO calculation of Lathan, Curtiss and Pople obtains the configuration (1) for the ground state of ethane, but they find that the energy of the $^2A_{1g}$ ionic state drops below that of the ^2E_g state when unrestricted open-shell SCF calculations are carried out for $C_2H_6^+$, some electron redistribution taking place when the geometry of the ion is optimized. These latter effects are of course neglected in Koopmans' theorem[10]. Murrell and

Schmidt[9], on the other hand, used an "equivalent orbital" treatment for correlation of ionization bands between various hydrocarbons, claiming that the $1e_g$ and $1e_u$ MOs of ethane should be symmetrically displaced about the $1t_2$ orbital of methane. However, as pointed out by Rabalais and Katrib[11] this rather doubtful procedure can yield different results depending on whether vertical or adiabatic ionization potentials are used for correlation.

The photoelectron spectrum of ethane has been reported by Hamrin et al.[12], Baker et al.[13], Narayan[14] and most recently by Rabalais and Katrib[11]. The first of these investigations, a rather low resolution experiment using X-rays[12], found a peak at a separation energy of 10.7eV which was assigned to the $3a_{1g}$ and $1e_g$ orbitals. The UPS experiments using resonance radiation[11,13,14] were able to resolve some structure in the overlapping $1e_g$ and $3a_{1g}$ bands. All these investigations assigned the ground state of $C_2H_6^+$ as ^2E_g, although the resolution exhibited in the earlier experiments[13,14] was insufficient to make a firm assignment based on the observed vibrational structure. The experiment of Rabalais and Katrib offers the best evidence for this assignment.

The photoelectron spectrum in the region of the overlapping $1e_g^{-1}$ and $3a_{1g}^{-1}$ bands is complicated by the Jahn-Teller effect, which splits the doubly degenerate $1e_g^{-1}$ (and $1e_u^{-1}$) state into two components.

The (e,2e) technique[1,2,15,16] enables one not only to determine electron separation energy spectra, as in photoelectron spectroscopy, but it also yields, to a very good approximation, the shapes and magnitudes of the square of the electronic momentum space wave functions, $\psi_i(q)$, for individual electronic orbitals. It also yields information on electron correlation effects and allows, in many instances, the unique definition of configuration interaction coefficients. It

therefore yields considerably more information on the structure of molecules than can be obtained with photoelectron spectroscopy. In particular, since the symmetries of the $3a_{1g}$ and $1e_g$ orbitals are quite different their momentum space wave functions should also be quite different, and therefore they should be easily distinguished in an (e,2e) experiment.

We report here a detailed investigation of the valence states of ethane using the noncoplanar symmetric (e,2e) reaction at both 400 and 1200eV.

2. EXPERIMENTAL PROCEDURE AND APPARATUS

The experiment was carried out using noncoplanar symmetric geometry in which the two electrons A and B have equal energies ($E_A = E_B = \frac{1}{2}E$) and are emitted at equal angles relative to the incident direction ($\theta_A = \theta_B = \theta$). The momentum transfer q to the ion is varied by varying the azimuth of one of the detectors, the azimuthal angle ϕ being defined so that the azimuthal angle between the two electrons is $\pi - \phi$. ϕ is therefore zero in the coplanar geometry. If the energy and momentum of the incident electron is E_o and $\underset{\sim}{k}_o$ respectively, the separation energy of the ejected electron is given by

$$\varepsilon = E_o - E = E_o - E_A - E_B \qquad (2)$$

whereas the recoil momentum of the ion is given by

$$\underset{\sim}{q} = \underset{\sim}{k}_o - \underset{\sim}{k}_A - \underset{\sim}{k}_B \qquad (3)$$

The magnitude of the recoil momentum, which is equal to the momentum of the target electron, is in the symmetric geometry given by

$$q = [(2k_A\cos\theta - k_o)^2 + 4k_A^2\sin^2\theta\sin^2\tfrac{1}{2}\phi]^{\frac{1}{2}} \qquad (4)$$

The experiment is therefore carried out in two modes. If the angles and the total energy E of the two final electrons are kept fixed and the incident energy is varied, separation energies of electrons ejected from orbitals in the target can be obtained. Keeping the energies fixed and varying the angle yields the cross section at different values of the bound electron momentum q. In the noncoplanar symmetric geometry (i.e. fixing θ and varying ϕ) the angular correlation so obtained is directly proportional to the square of the momentum space wave function of the ejected electron [1,15,16].

A schematic diagram of the apparatus is shown in figure 1. It is similar to an earlier version described in references [1] and [15]. Since a detailed description of the apparatus is given in reference 16 only a brief summary will be given here.

The electron spectrometer consists of two cylindrical mirror analyzers mounted so that the entrance angle (θ) relative to the incident beam is 42.3^{o}. The incident beam is produced by an electron gun with a tungsten hairpin filament. Alignment with the interaction region is achieved by means of two orthogonal pairs of deflection plates. The gun and deflection plates are surrounded by a stainless steel tube with an exit aperture to shield the interaction region from stray electrons and electrostatic fields. Focusing of the electron beam is carried out with the aid of the Faraday cup by maximising the ratio of the current through the cup aperture to the current collected on the aperture plate.

The molecular beam enters the interaction region through a non-magnetic steel nozzle of inner diameter 0.25mm. The high purity gas samples are first passed through a trap and then leaked into the interaction region through a variable leak valve. The background pressure is of the order of 5×10^{-7} torr and this rises to approximately 10^{-5} torr when the gas beam is on. The pressure in the interaction region is

of the order of 10^{-3} torr.

The electrons enter the two cylindrical mirror analyzers through a retarding lens system. These three stage cylindrical retarding lenses decelerate the electrons and focus them on the entrance apertures of the analyzers. The full acceptance angle of each analyzer is approximately 4^{o}. A channel electron multiplier (CEM) is mounted behind the exit aperture of each analyzer. A grid in front of the CEM's can be biased to prevent very low energy secondary electrons from entering the CEM's. One of the analyzers (on the left in figure 1) is fixed, the other analyzer being rotated about the incident beam direction by a chain drive connected to a rotatable feedthrough driven by a stepping motor outside the vacuum chamber.

The energy resolution obtained in the coincidence experiments is a convolution of the two analyzer functions and the energy distribution of the electron beam. It also depends on the decelerating ratio of the lens. This resolution, as well as the separation energy scale, is measured directly by using helium as a calibration gas.

The choice of noncoplanar scattering geometry has several experimental advantages as well as some theoretical ones[16]. The main advantage is that the angular correlation must be symmetric about $\phi = 0^{o}$, and the count rates in each CEM must be independent of the angular setting.

The earth's magnetic field is nulled by Helmholtz coils outside the vacuum system as well as by mu-metal lining inside the vacuum system. Care is taken to use only nonmagnetic materials in the construction of the apparatus.

In order to select the significant (e,2e) events it is necessary to discriminate against other events by using a fast coincidence technique. A schematic diagram of the signal processing and recording electronics is shown in figure 2.

The pulses from the CEM's are fed to double delay line amplifiers (DDL) through preamplifiers, the amplified bipolar pulses triggering fast timing discriminators which operate in the cross over pick-off mode. One of the fast discriminator pulses is used as the start pulse for a time to amplitude converter (TAC), the pulse from the other discriminator is delayed and fed to the stop input of the TAC. The time delay spectrum from the output of the TAC is fed simultaneously to two single channel analyzers and a multi-channel analyzer which is used for setting up and monitoring the experiments. The window of one SCA is set over the coincidence peak, whereas the window of the second SCA is set to record accidental events, the background window width being ten times that of the coincidence window in order to reduce statistical uncertainties. Timing resolutions are typically of the order of 5-10 nanoseconds. The pulses from the two SCA's are counted by scalers online to a PDP 8/L computer. A third scaler recording the counts from the movable analyzer operates in a preset mode. It therefore corrects for any small variation in the electron current or the target gas density, as well as any small variation in the efficiency of the detector with the angular setting.

The data recording is fully automated and the apparatus can be controlled by the online computer. A machine language program allows measurement of either the binding energy spectra or angular correlations. In both cases the full range of the appropriate variable can be rapidly scanned in order to eliminate errors due to long term drifts. The progress of the experiment can be monitored on a real time display on a storage oscilloscope.

During any experimental run the energies of the outgoing electrons are kept fixed at equal values. In the separation energy mode the energy of the primary beam is varied by means of a programmable power supply. For the angular correlation measurements the incident energy is adjusted for the appropriate separation energy, and the azimuthal angular

setting of one of the analyzers changed by the computer controlled stepping motor drive.

3. THEORETICAL BACKGROUND

The theory of the (e,2e) reaction on molecules has been investigated in some detail[16-19]. The Born-Oppenheimer approximation is made, namely each many body wave function is considered as a product of rotational, vibrational, and electronic wave functions. Since the target gas is at some finite temperature, it is in one of an ensemble of rotational states given by the Boltzmann distribution. Since the (e,2e) cross section is, however, independent of the total angular momentum of the molecular state [16-19], the sum over initial rotational states is trivial. The target molecule is usually considered to be in the ground vibrational state.

The expression for the cross section can be greatly simplified by applying the closure relation for the final rotational and vibrational states, i.e. summing over all final vibrational and rotational states. In this case the cross section in the eikonal distorted wave off-shell impulse approximation is given by

$$\sigma \propto R|T|^2 \sum_{u_r} \langle O|\left|d\Omega(2\pi)^{-3}\right|\int d^3r \exp(i\underline{q}.\underline{r})(F|G\rangle|^2|O\rangle \qquad (5)$$

where the integral indicated by Dirac brackets is an average over the ground state vibrations and the integral over Ω is the rotational integral. $|G\rangle$ and $|F)$ are the electronic eigenstates of the molecule and ion respectively. R is an attenuation factor which depends on the absorption of the electron waves and T is the half off-shell Coulomb t-matrix element which describes the "off-shell" free electron-electron collision cross section. In the noncoplanar geometry $|T|^2$ is independent of the angle ϕ. At high enough energies we can make the plane wave

approximation and the attenuation factor R is independent of the separation energy ε of the ejected electron.

This expression has been thoroughly checked[20] for the simplest molecular target, H_2 and D_2, where it was shown that the average over the initial vibrational motion can be replaced by the equilibrium distance value. The (e,2e) cross section then depends only on the square of the Fourier transform of the overlap integral $\langle F|G\rangle$.

The molecular independent particle states $|\alpha\rangle$ which define the basis for the electronic eigenstates $|F\rangle$ and $|G\rangle$ are usually expressed in terms of the LCAO picture. Each molecular orbital $\psi_j(\underline{r}',R')$ in the determinant $|\alpha\rangle$ is written as a sum of terms centered at each atom centre $\underline{R}'_s$, each term having angular properties given by a spherical harmonic $Y_{\ell m}(\underline{r}'-\underline{R}'_s)$

$$\psi_j(\underline{r}',R') = \sum_s \psi_s^{(j)}(\underline{r}'-\underline{R}'_s) \tag{6}$$

$$\psi_s^{(j)}(\underline{r}) = \sum_{\ell m} u_{\ell m}^{(s)}(r) Y_{\ell m}(\hat{\underline{r}}) \tag{7}$$

The electronic states $|F\rangle$ and $|G\rangle$ are in general given by structure calculations as configuration interaction expansions of the independent particle states. The overlap integral is then given by[16]

$$\langle F|G\rangle = \sum_{j\alpha} a_\alpha^{(G)} t_{j\alpha}^{(F)} C_{jr\alpha} \psi_j(\underline{r}',R') \tag{8}$$

where the fractional parentage coefficient is the product of the configuration interaction coefficients a and t, which refer to the initial molecular and final ion states respectively, and $C_{jr\alpha}$ is a Clebsch-Gordan coefficient of the molecular point group. For "closed shell" target molecules it is reasonable to assume the Hartree-Fock approximation for the target. For ethane the nearest unoccupied orbitals are the $3a_{2u}$, $4a_{1g}$, $2e_g$ and $2e_u$ orbitals with excitation energies in the approximate range of 7-10eV[21]. The energy "gap"

between configuration (1) and any configuration with $^1A_{1g}$ symmetry arrived at by elevating a pair of electrons from configuration (1) to any of the above unoccupied orbitals, is therefore of the order of 40eV. Such configurations are therefore likely to be small in the CI expansion of the groundstate of ethane. In the target Hartree-Fock approximation $a_o = 1$ and all other a_α's are zero, and therefore

$$(F|G> = n_r^{\frac{1}{2}} t_{co}^{(F)} \psi_c(\underline{r}',R') \qquad (9)$$

where n_r is the dimension of the representation of the point group r. The characteristic orbital ψ_c is the one which couples to the target groundstate $\alpha = 0$ in the configuration-interaction expansion of the ion state $|F)$. The (e,2e) cross section is then given by

$$\sigma \propto S_c^{(F)} n_r |T|^2 \sum_{nm} \int d\hat{q} \phi_n^*(\underline{q},R_{nm}) \phi_m(\underline{q},R_{nm}) \exp[i\underline{q}.(\underline{R}_m - \underline{R}_n)] \qquad (10)$$

where $S_c^{(F)} = |t_{co}^{(F)}|^2$ is the spectroscopic factor for the state to contain the orbital c, R_{nm} is the set of equilibrium distances between the nth and mth nucleus, and the momentum space wave function is

$$\phi_n(\underline{q},R) = (2\pi)^{-3/2} \int d^3r \exp(i\underline{q}.\underline{r}) \psi_n(\underline{r},R) \ , \qquad (11)$$

where ψ_n is the sum of all the atomic functions entered on the nucleus n in the LCAO for the characteristic orbital. In the noncoplanar symmetric geometry the (e,2e) cross section is therefore proportional to the spectroscopic factor for the ion state to contain the particular molecular orbital, and also to a factor which depends on the product of the atom centered momentum space wave functions averaged over all directions.

Relative magnitudes for ion eigenstates F are governed by the sum rule

$$\sum_F S_c^{(F)} = 1 \ , \qquad (12)$$

which states that the full spectroscopic strength for each hole state c

must be distributed over the eigenstates F. The sum rule is slightly modified when two hole configurations may interact in the same representation, such as $2a_{1g}^{-1}$ and $3a_{1g}^{-1}$. However this interaction is small.

In evaluating the expression (10) all the relevant terms λ_u in the spherical harmonic expansion of the exponential factor are included. We have not made the simplifying approximation $\lambda = 0$ that was used in references 17 and 18.

4. RESULTS AND DISCUSSION

The separation energy spectra obtained at E = 400eV and at different values of the azimuthal angle ϕ, i.e. of q, are shown in figures 3 and 4. The 0^o and 10^o spectra in figure 3 show the separation energy peaks due to all of the five valence orbitals of ethane. These are, in order of increasing separation energy, the $1e_g$, $3a_{1g}$, $1e_u$, $2a_{2u}$ and $2a_{1g}$ orbitals. As we pointed out in the introduction, the $3a_{1g}$ and $1e_u$ orbitals overlap to a large extent. In order to separate these orbitals it is therefore necessary to deconvolute the spectra. This also applies to the $1e_u$ orbital which was not completely resolved from the $3a_{1g}$ orbital.

The deconvolution procedure is greatly simplified by the fact that the angular correlations of the $1e_g$ and $3a_{1g}$ orbitals are expected to be quite different. The contribution of the $3a_{1g}$ orbital should be a maximum at 0^o whereas that of the $1e_g$ orbital should be a minimum at that angle. As the angle is increased the relative contribution of the $1e_g$ state should also increase, reaching a maximum at approximately 15^o. This can be seen by inspection of the separation energy spectra in figures 3 and 4. The shape of the spectra in the region 10-17 eV changes quite markedly as the angle ϕ increases from 0 to 25^o.

The energy resolution at 400 eV is determined from helium energy spectra to be 1.5 eV FWHM, the instrumental resolution being well approximated by a Gaussian. The shape of the $1e_u$ ionization peak has been quite well determined by photoelectron spectroscopy [11]. Its width is of the order of 1.2 eV. The shape of the $1e_g$ ionization peak is expected to be similar to the $1e_u$ peak. On the other hand the $3a_{1g}$ peak, which does not suffer Jahn-Teller splitting, is likely to be narrower. Although the $1e_g$ peak is not intrinsically Gaussian in shape, when it is folded into the broader Gaussian experimental resolution function the result is very close to a Gaussian shape. Therefore in the deconvolution procedure, which was carried out on a PDP-11 computer, only Gaussians were used. The widths of the Gaussians required to obtain optimal fits are consistent with the known experimental resolution and the available data on the band structures[11-14]. Figures 3 and 4 show the fits obtained at the various angles.

The vertical ionization potentials obtained from these fits are given in table 1. The $1e_g$ and $3a_{1g}$ orbitals are identified by their angular correlations. These will be discussed shortly. Also included in table 1 are the vertical ionization energies obtained in various photoelectron spectroscopy experiments[11-14], and the results of two MO calculations[7,21]. The agreement between the present results and the most recent UPS work of Rabalais and Katrib is quite good.

The separation energy spectra obtained at 1200 eV and at $\phi = 0^o$ and 7^o are shown in figure 5. The positions of the $1e_u$, $3a_{1g}$, $1e_g$, $2a_{2u}$ and $2a_{1g}$ peaks are indicated in the figure by arrows, the resolution being too poor to cleanly resolve any of these states. The data does, however, show a considerable amount of structure above $\varepsilon = 29$eV, which must be due to configuration interaction effects. This structure extends all the way to $\varepsilon \approx 55$eV.

The momentum distributions obtained at 400eV, and also at 1200eV for the $2a_{2u}$ and $2a_{1g}$ orbitals, are shown in figure 6. Although absolute cross sections are not measured, the experiment does obtain the relative magnitudes of the various cross sections, and these are as shown in figure 6. They are compared with the relative cross section magnitudes and shapes calculated with the plane wave theory and the orbital wave functions of Snyder and Basch. The agreement is remarkably good. When the finite angular resolution (4^{o}) is allowed for, the agreement at low q is considerably improved (dashed curve).

The summed cross section for the high energy structure ($\varepsilon > 29$eV) also depends on the angle. The cross section at 7^{o} ($q \approx 0.6$a.u.) being only 0.6 ± 0.1 times the value at 0^{o} ($q \approx 0.3$a.u.). This means that at least 35% of the high energy structure must belong to the $2a_{1g}^{-1}$ configuration, since none of the other angular correlations decrease sufficiently rapidly with q. This means that the $2a_{1g}$ cross section determined by summing over the peak at 24.5 eV must be multiplied by a factor of at least 1.22. This correction has been included in the data shown in figure 6. The $2a_{1g}$ cross section may be even larger depending on the relative contributions of the $1e_{u}$, $1e_{g}$, $2a_{2u}$ and $3a_{1g}$ orbitals to the high energy structure.

The angular correlations observed at ε = 33, 38, 42.5, and 48eV are shown in figure 7. The structure at ε = 33eV can be fitted quite well by the $2a_{1g}$ angular correlation (solid curve). At the higher separation energies there is, however, considerable excess of high q components, although the majority of the structure can still be attributed to the $2a_{1g}$ orbital. At ε = 48eV the $3a_{1g}$ orbital could be making the dominant contribution. From the momentum distributions shown in figure 7, it appears likely that the contribution of the $2a_{1g}$ orbital to the high energy structure is considerably greater than the minimum value of 35% estimated from the 0^{o} and 7^{o} energy spectra.

If the contribution is as high as 70%, it means that the cross section of the 24.5eV peak must be increased by 45% rather than by 22%. This would considerably improve the agreement with the calculated cross section at low q, where the cross section is large.

The $1e_g$ and $3a_{1g}$ momentum distributions are obtained by two independent means. The first is to compare the deconvoluted peak areas with the $1e_u$ cross section. This can be measured on the high energy side of its peak, where there is negligible overlap with the other states. The $1e_g$ angular correlation is also obtained by sitting on the low energy side of the $1e_g$ peak, where overlap from the $3a_{1g}$ state is negligible. The second method used for measuring the $3a_{1g}$ momentum distribution is to measure the angular correlation at ϵ = 13.8eV and then to correct for the amount of overlap expected from the $1e_g$ and $1e_u$ states on the basis of the deconvoluted energy spectra. The resulting angular correlations (fig. 6) are in quite good agreement with theory, both in shape and magnitude, and obviously remove any possible doubt about the identification of these orbitals.

The photoelectron studies by Baker et al.[13], Narayan[14] and Rabalais and Katrib[11] agree with our transition assignments, but they differ in their interpretation of the vibrational structure on which their assignments are based.

Finally we would like to make a comment about the comparison of the measured and calculated separation energies reported in table 1. The MO values, obtained by means of Koopmans theorem[10], are consistently higher than the separation energies we observed for the main peaks belonging to the various valence orbitals. However, the separation energy for the hole state is defined as the centroid of all of the ion eigenstates containing the hole state configuration. The high energy configuration interaction structure shown in figures 5 and 7 therefore serves to increase the experimental separation energies,

and in particular that of the $2a_{1g}$ orbital.

5. CONCLUSIONS

The present (e,2e) results on ethane confirm the molecular orbital assignments derived from molecular H.F. calculations. They further show that the M.O. calculations describe quite accurately the momentum distributions of electrons in a given orbital. The relative magnitudes of the different cross sections are also well described by the plane wave theory.

In order to describe relative magnitudes of cross sections, one must sum the contributions to a particular hole state over all the ion eigenstates which contain that hole state. With the present resolution this cannot be done uniquely for the ion eigenstates above 29eV, although the angular correlations for these states and the sum rule for relative magnitudes give strong evidence for the assignment. Comparison of centroid separation energies with M.O. calculations gives further information on this point. The complete description of the separation energy structure above 29eV requires accurate CI calculations of the ground state of the neutral ethane molecule as well as of the ion eigenstates. Calculated CI coefficients can then be compared with the experimental spectroscopic factors. Although it is a reasonable approximation to assume the Hartree-Fock approximation for the target[16], this needs to be checked by detailed calculations.

The (e,2e) spectroscopy must be contrasted with photoelectron spectroscopy, which provides details of the energy levels of ions and some clues about the assignment of the levels containing most of the spectroscopic strength to representations of the molecular point group. (e,2e) spectroscopy provides unequivocal assignments, not only of the main peaks, but potentially (and to some extent actually at present) of the smaller peaks. In addition it tests the shapes of the molecular

orbitals and the magnitudes of the spectroscopic factors S_c^F, capabilities for which it is unique.

ACKNOWLEDGMENT

We are grateful to the Australian Research Grants Committee for financial support.

REFERENCES

[1] S.T. Hood, E. Weigold, I.E. McCarthy and P.J.O. Teubner, Nature Physical Science, 245, No. 144 (1973) 65.

[2] E. Weigold, S. Dey, A. Dixon, I.E. McCarthy and P.J.O. Teubner, Chem. Phys. Lett. (to be published).

[3] W.E. Palke and W.N. Lipscomb, J. Am. Chem. Soc., 88 (1966) 2384.

[4] E. Clementi and D.R. Davis, J. Chem. Phys. 45 (1966) 2593.

[5] A. Veillard, Chem. Phys. Lett. 3 (1969) 128, 565.

[6] W. Fink and L.C. Allen, J. Chem. Phys. 46 (1967) 2261.

[7] R. Clementi and H. Popkie, J. Chem. Phys. 57 (1972) 4870.

[8] W.A. Latham, L.A. Curtiss and J.A. Pople, Molec. Phys. 22 (1971) 1081.

[9] J.N. Murrell and W. Schmidt, J. Chem. Soc. Faraday Trans. 68, (1972) 1709.

[10] T. Koopmans, Physica 1 (1934) 104.

[11] J.W. Rabalais and A. Katrib, Molec. Phys. 27 (1974) 923.

[12] K. Hamrin, G. Johannsson, U. Gelius, A. Fahlman, C. Nordling and K. Siegbahn, Chem. Phys. Lett. 1 (1968) 613.

[13] A.D. Baker, C. Baker, C.R. Brundle and D.W. Turner, Int. J. Mass. Spectrosc. Ion Phys., 1 (1968) 285.

[14] B. Narayan, Molec. Phys., 23 (1972) 281.

[15] E. Weigold, S.T. Hood and P.J.O. Teubner, Phys. Rev. Lett. 30 (1973) 475.

[16] I.E. McCarthy and E. Weigold, Physics Reports (to be published).

[17] I.E. McCarthy, J. Phys. B.: Atom. Molec. Phys. 6 (1973) 2350.

[18] I.E. McCarthy, J. Phys. B.: Atom. Molec. Phys. 8 (1975) 2133.

[19] V.G. Levin, V.G. Neudatchin, A.V. Pavlitchenkov and Yu. F. Smirnov, J. Chem. Phys. 63 (1975) 1541.

[20] S. Dey, I.E. McCarthy, P.J.O. Teubner and E. Weigold, Phys. Rev. Lett. 34 (1975) 782.

[21] L.C. Snyder and H. Basch, "Molecular Wave Functions and Properties" (Wiley, N.Y. 1972).

TABLE 1

The vertical ionization potentials in eV of the main peak for the valence orbitals of ethane as measured by (e,2e) and photoelectron spectroscopy compared with several MO calculations.

Orbital	(e.2e) (present work)	XPS 12*	UPS 11*	UPS 13*	UPS 14*	MO calculations 7*	MO calculations 21*
$1e_g$	12.25 ± 0.1	10.7	12.4	~12.5	~12	13.2	13.1
$3a_{1g}$	13.35 ± 0.1		13.5	~13.5	~13	13.8	13.5
$1e_u$	15.45 ± 0.1	14.7	15.4	~15.5	~15.5	16.1	16.2
$2a_{2u}$	21.0 ± 0.1	20.3	20.4	~20.5	-	22.9	22.7
$2a_{1g}$	24.5 ± 0.1	23.9	24	-	-	27.5	27.6

* Reference number.

FIGURE CAPTIONS

Fig. 1. The noncoplanar symmetric coincidence spectrometer. 1 - the rotatable cylindrical mirror analyzer; 2 - the stationary cylindrical mirror analyzer; 3 - electron gun; 4 - deflection plates; 5 - gas beam inlet tube; 6 - Faraday cup; 7 - three stage cylindrical decelerating lenses; 8 - channel electron multipliers; 9 - feed-through drive for rotatable spectrometer (1).

Fig. 2. Schematic diagram of electronic circuitry.

Fig. 3. The differential cross section for the 400eV (e,2e) reaction on C_2H_6 at $\phi = 0^\circ$, 10°, and 15° (inset) plotted against the separation energy. The valence orbitals to which the various separation energy peaks are assigned are indicated by the arrows. The curves show the spectra obtained on deconvoluting the data using the procedure discussed in the text.

Fig. 4. The differential cross section for the 400eV (e,2e) reaction on C_2H_6 at $\phi = 3^\circ$, 6°, 19° and 25° plotted against the separation energy. The curves show the deconvoluted $1e_g$, $3a_{1g}$, and $1e_u$ contributions.

Fig. 5. The differential cross section for the 1200eV (e,2e) reaction on C_2H_6 at $\phi = 0^\circ$ and 7° plotted against the separation energy. The separation energies of the principal $1e_u$, $3a_{1g}$, $1e_g$, $2a_{2u}$, and $2a_{1g}$ contributions are indicated by arrows. The broken arrows indicate the

additional separation energies at which angular correlations are reported (fig. 7).

Fig. 6. The relative noncoplanar symmetric differential cross sections for the ejection of electrons from the valence orbitals of ethane plotted as a function of the recoil momentum q. The open and filled symbols show respectively the 400eV and 1200eV cross sections. The solid lines are the plane wave cross sections calculated using the orbital wave functions of Snyder and Basch[21]. They are normalized to the data at one point only, the $1e_u$ cross section at $q \simeq 0.6$ a.u. The dashed lines show the effect of including the finite acceptance angles in the calculations.

Fig. 7. The 400eV (open circles) and 1200eV (filled circles) noncoplanar symmetric differential cross sections, at separation energies of 23, 38, 42.5 and 48eV, plotted against the recoil momentum g. The solid and dashed curves show respectively the shapes of the $2a_{1g}$ and $3a_{1g}$ cross sections calculated using the orbital wave functions of Snyder and Basch[21].

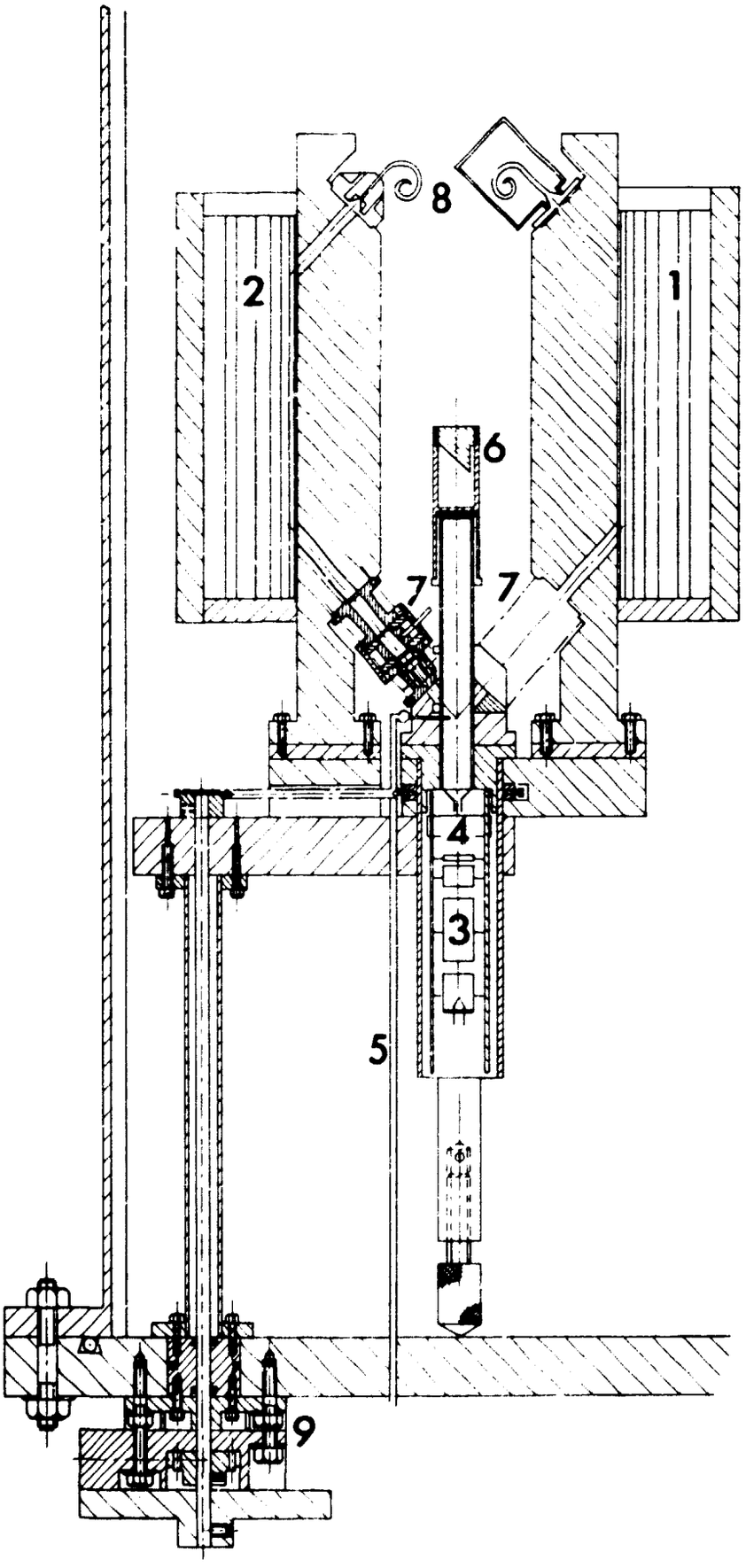

Figure 1.

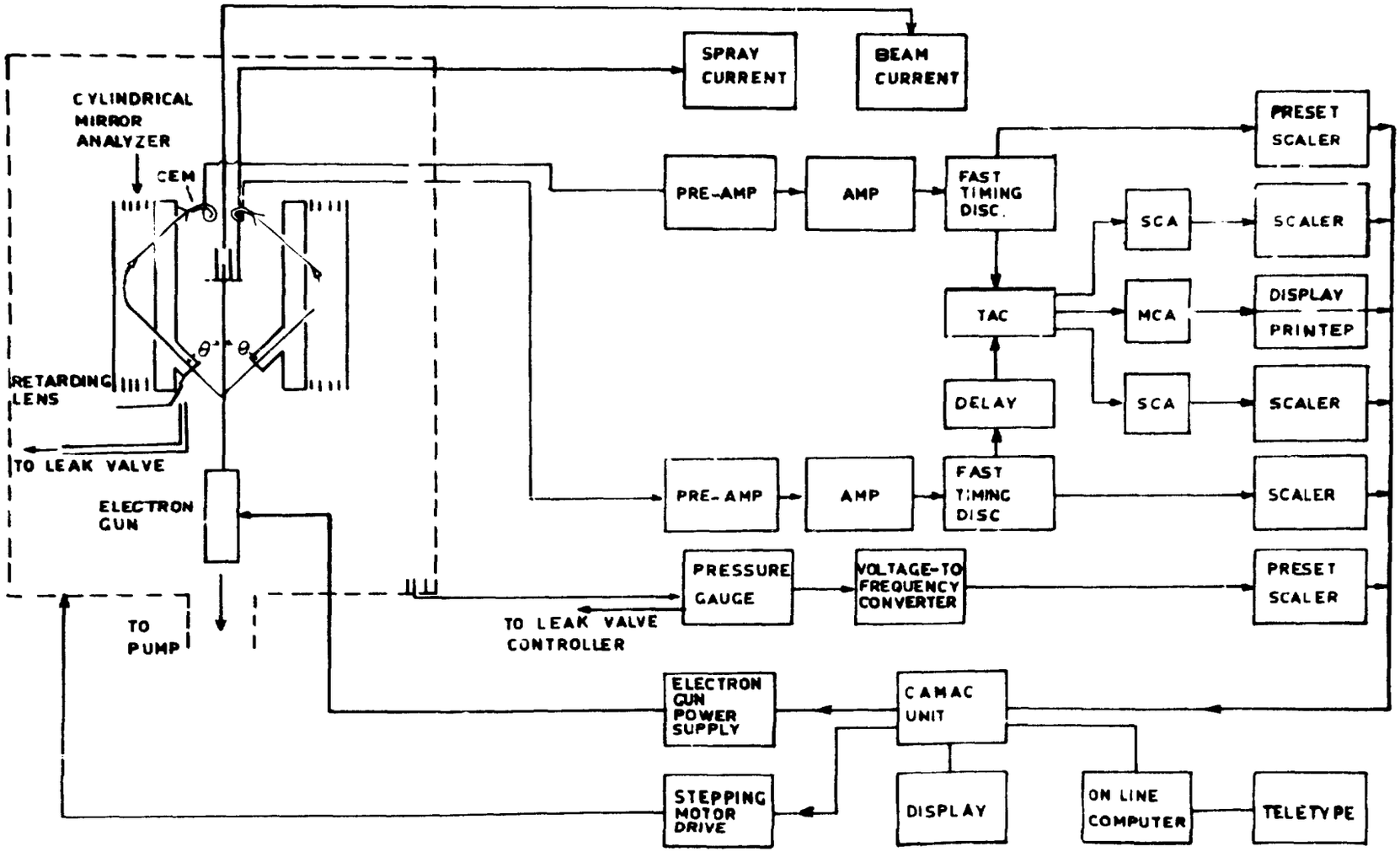
CYLINDRICAL MIRROR ANALYZER
CEM
RETARDING LENS
TO LEAK VALVE
ELECTRON GUN
TO PUMP
SPRAY CURRENT
BEAM CURRENT
PRE-AMP
AMP
FAST TIMING DISC.
PRESET SCALER
SCA
SCALER
TAC
MCA
DISPLAY PRINTEP
DELAY
SCA
SCALER
PRE-AMP
AMP
FAST TIMING DISC
SCALER
PRESSURE GAUGE
VOLTAGE-TO FREQUENCY CONVERTER
PRESET SCALER
TO LEAK VALVE CONTROLLER
ELECTRON GUN POWER SUPPLY
CAMAC UNIT
STEPPING MOTOR DRIVE
DISPLAY
ON LINE COMPUTER
TELETYPE

Figure 2.

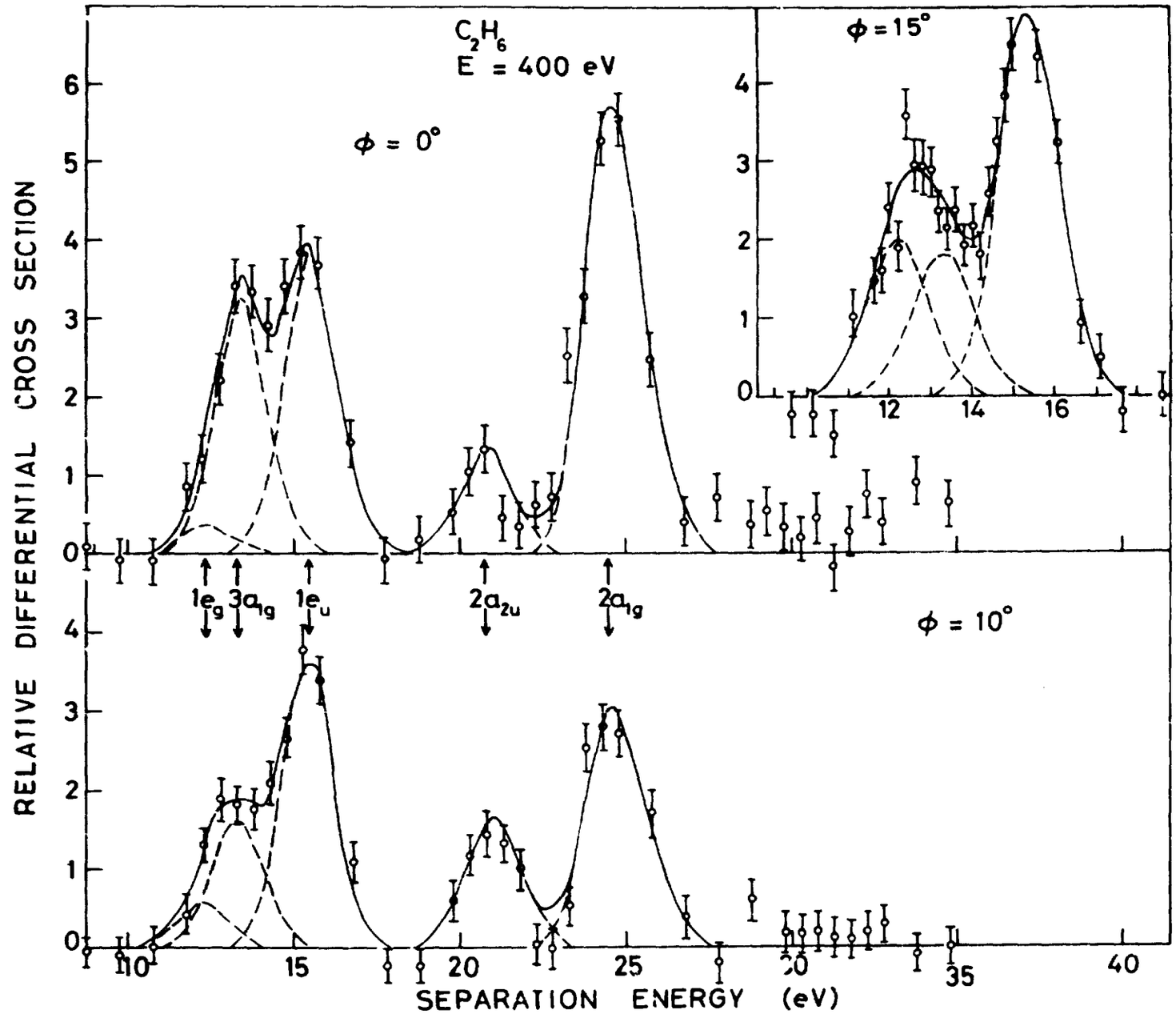
C_2H_6
E = 400 eV
ϕ = 0°
ϕ = 15°
ϕ = 10°
RELATIVE DIFFERENTIAL CROSS SECTION
SEPARATION ENERGY (eV)
$1e_g$ $3a_{1g}$ $1e_u$ $2a_{2u}$ $2a_{1g}$

Figure 3.

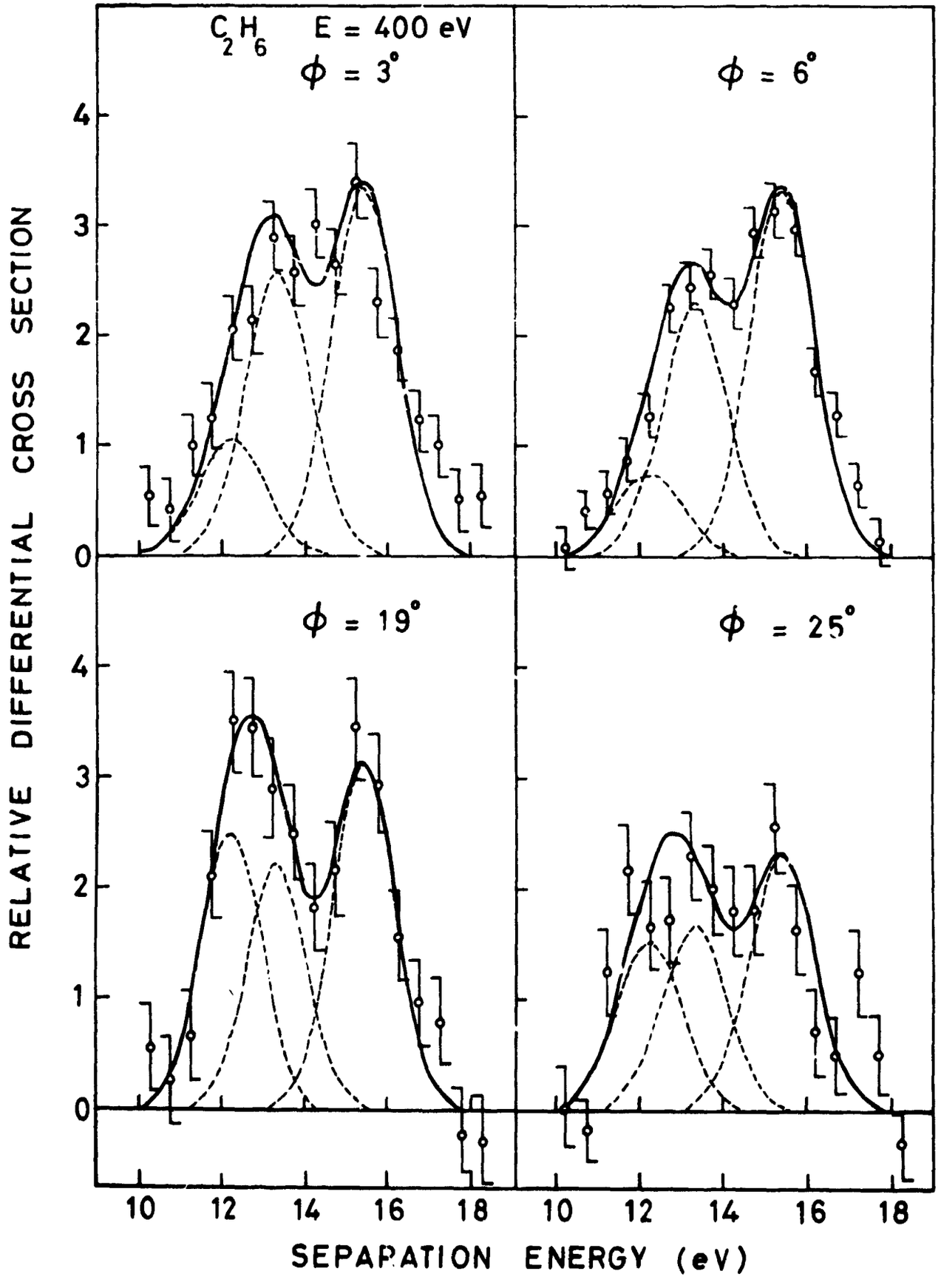
C2H6 E = 400 eV
ϕ = 3°
ϕ = 6°
ϕ = 19°
ϕ = 25°
RELATIVE DIFFERENTIAL CROSS SECTION
SEPARATION ENERGY (eV)
0
1
2
3
4
10
12
14
16
18

Figure 4.

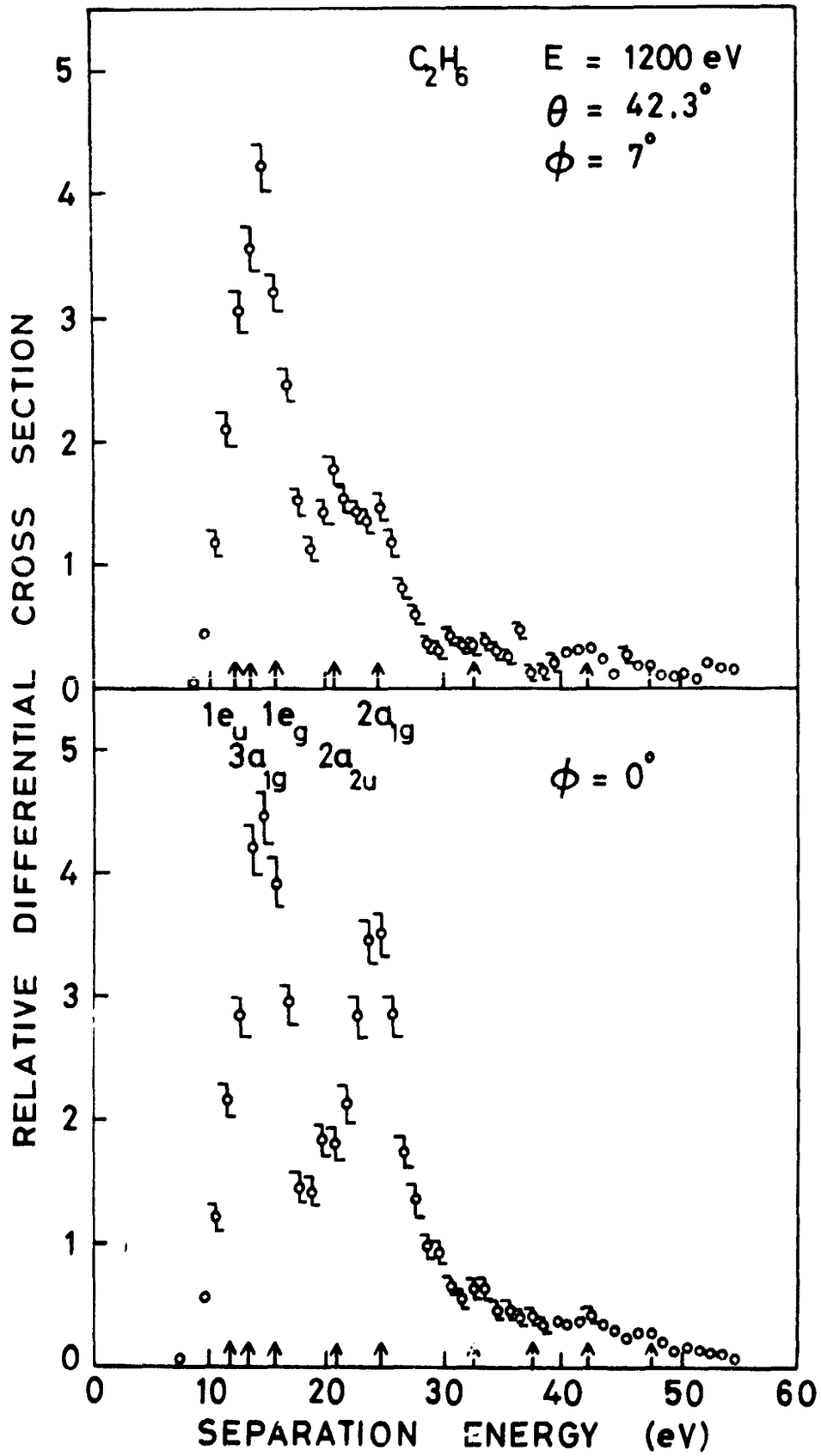
C_2H_6
E = 1200 eV
θ = 42.3°
φ = 7°
φ = 0°
$1e_u$
$1e_g$
$2a_{1g}$
$3a_{1g}$
$2a_{2u}$
RELATIVE DIFFERENTIAL CROSS SECTION
SEPARATION ENERGY (eV)
0
1
2
3
4
5
10
20
30
40
50
60

Figure 5.

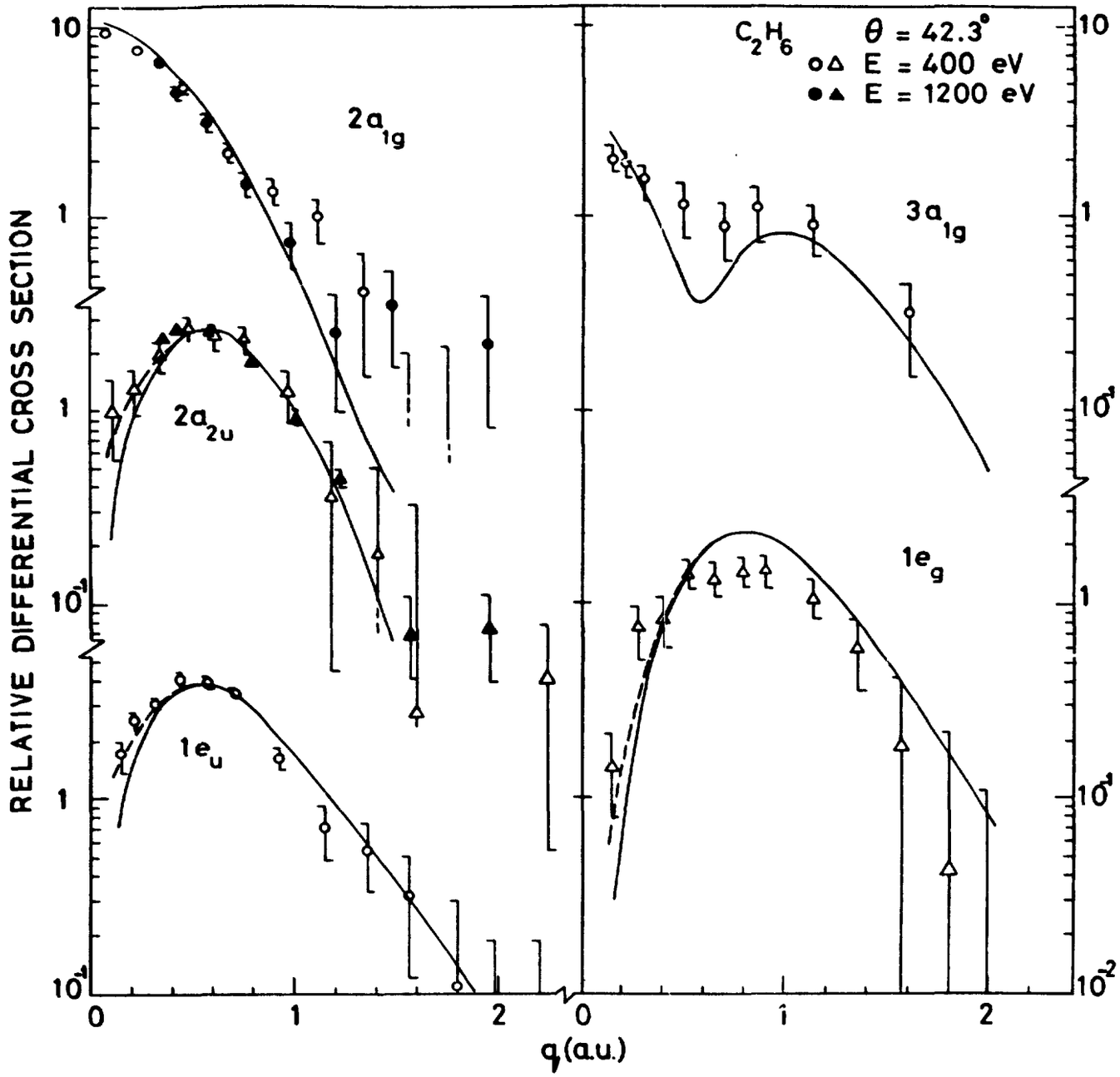
C_2H_6
θ = 42.3°
E = 400 eV
E = 1200 eV
$2a_{1g}$
$3a_{1g}$
$2a_{2u}$
$1e_g$
$1e_u$
RELATIVE DIFFERENTIAL CROSS SECTION
q(a.u.)

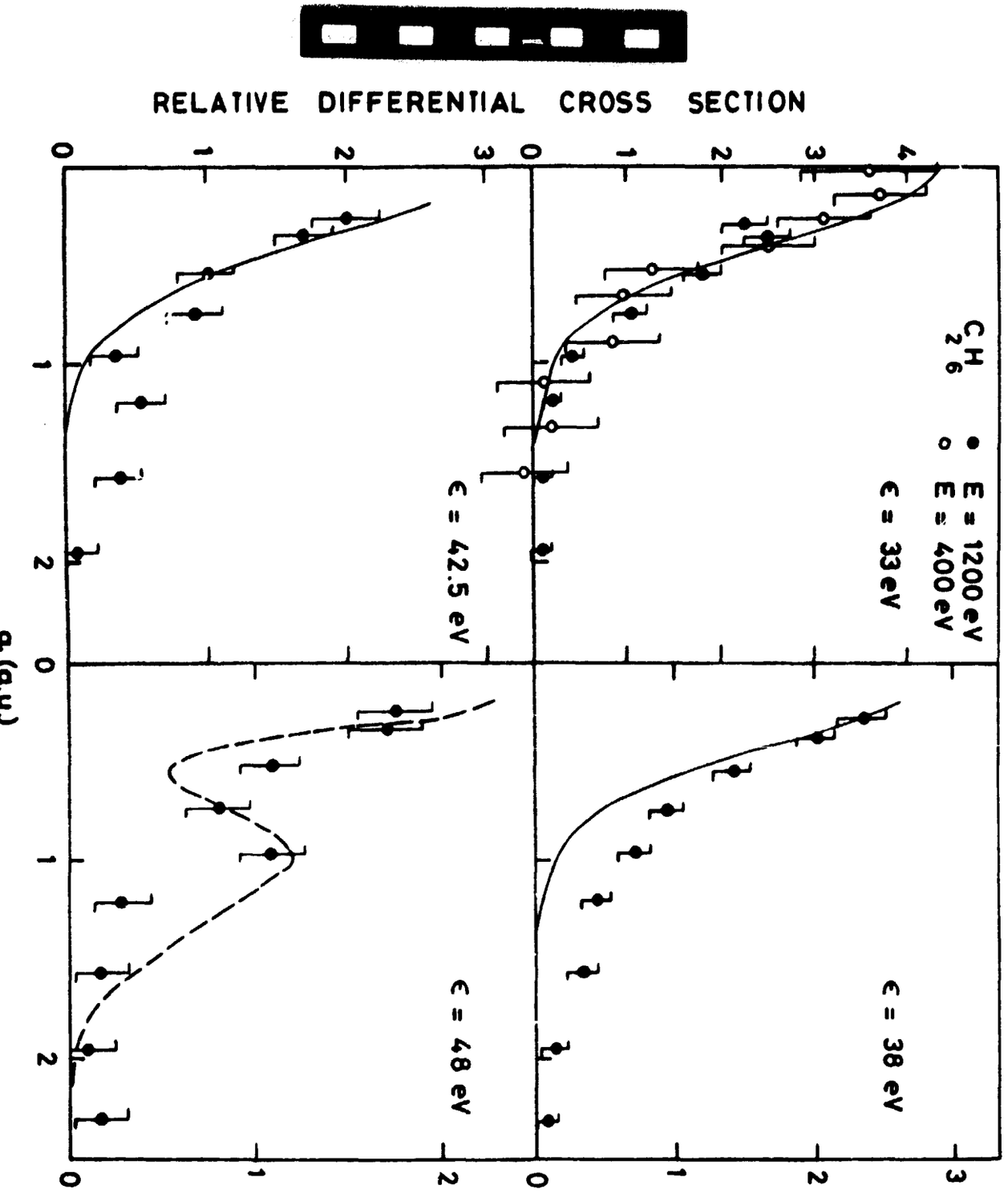
RELATIVE DIFFERENTIAL CROSS SECTION
C_2H_6
● E = 1200 eV
○ E = 400 eV
ε = 33 eV
ε = 42.5 eV
ε = 38 eV
ε = 48 eV
q (a.u.)

Figure 7.